


**Phase-sensitive thermoelectricity and long-range Josephson effect supported by thermal gradient**Mikhail S. Kalenkov *I. E. Tamm Department of Theoretical Physics, P. N. Lebedev Physical Institute, 119991 Moscow, Russia*

Pavel E. Dolgirev

*Department of Physics, Harvard University, Cambridge Massachusetts 02138, USA*Andrei D. Zaikin *Institute for Quantum Materials and Technologies, Karlsruhe Institute of Technology (KIT), 76021 Karlsruhe, Germany  
and National Research University Higher School of Economics, 101000 Moscow, Russia*

(Received 27 November 2019; revised manuscript received 13 April 2020; accepted 15 April 2020; published 8 May 2020)

We demonstrate that a temperature gradient can strongly stimulate the thermoelectric signal, as well as dc Josephson current, in multiterminal superconducting hybrid nanostructures. At temperatures  $T$  sufficiently exceeding the Thouless energy of our device, both the supercurrent and the thermoinduced voltage are dominated by the contribution from nonequilibrium low-energy quasiparticles and are predicted to decay slowly (algebraically rather than exponentially) with increasing  $T$ . We also predict a nontrivial current-phase relation and a transition to a  $\pi$ -junction state controlled by both the temperature gradient and the system topology. All these features are simultaneously observable in the same experiment.

DOI: [10.1103/PhysRevB.101.180505](https://doi.org/10.1103/PhysRevB.101.180505)

Superconducting hybrid structures exposed to a temperature gradient acquire a variety of intriguing properties. One of them is the thermoelectric effect [1] implying the presence of thermoinduced electric currents and/or voltages inside the sample. At low temperatures, these thermoelectric signals are *phase coherent*, which results in their periodic dependence on the phase of a superconducting condensate. Thermoelectricity gives rise to diverse applications ranging from thermometry and refrigeration [2] to phase-coherent caloritronics [3], paving the way to an emerging field of thermal logic [4] operating with information in the form of energy.

Superconducting circuits appropriate for such applications may involve superconducting-normal-superconducting (SNS) junctions of different geometries. In such structures, low-temperature electron transport is strongly influenced by the proximity effect implying penetration of superconducting correlations deep into the normal metal. As a result, macroscopic quantum coherence is established across the whole structure, thus supporting the Josephson current  $I_J$  between superconducting terminals.

In equilibrium, the magnitude of this effect essentially depends on the relation between temperature  $T$  and an effective Thouless energy  $E_{\text{Th}}$  of an SNS device. As soon as  $T$  strongly exceeds  $E_{\text{Th}}$ , the supercurrent reduces exponentially  $I_J \propto e^{-\sqrt{2\pi T/E_{\text{Th}}}}$  [5,6], and hence long-range phase coherence gets effectively suppressed at such values of  $T$ . A similar conclusion concerning the magnitude of the thermoelectric voltage signal  $V_T$  could be extracted from many previous theoretical studies [7–9].

In this Rapid Communication, we will demonstrate that by exposing the system to a temperature gradient, one can effectively support long-range phase coherence at temperatures strongly exceeding the Thouless energy  $E_{\text{Th}}$  where the equilibrium supercurrent becomes negligible.

Consider a long SNS junction with normal-state resistance  $R_n$  and two extra normal terminals attached to the central N wire as shown in Fig. 1. Provided these normal terminals are maintained at different temperatures  $T_1$  and  $T_2$ , the electron distribution function inside the junction is driven out of equilibrium. Below we are going to demonstrate that in the limit  $T_{1,2} \gg E_{\text{Th}}$  the Josephson critical current  $I_C$ —up to some geometry factors—takes the form

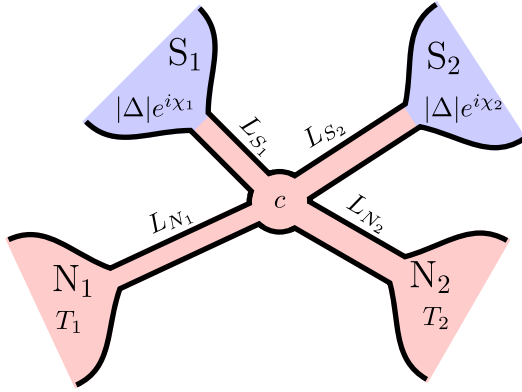
$$I_C \sim E_{\text{Th}}^2 |1/T_1 - 1/T_2| / (eR_n), \quad (1)$$

thus being a lot bigger than the equilibrium current  $I_J$  at any of the two temperatures  $T_1$  or  $T_2$ . Also, in this regime, the system is described by a nonsinusoidal current-phase relation (CPR) and may exhibit a pronounced  $\pi$ -junction-like behavior.

Furthermore, below we will show that, depending on its topology, the system can develop a large phase-coherent thermoelectric voltage signal that *does not* decay exponentially even if temperature increases above  $E_{\text{Th}}$ . Remarkably, at  $T_{1,2} \gg E_{\text{Th}}$ , the magnitude of this signal  $V_T$  turns out to have exactly the same temperature dependence as  $I_C$ , i.e.,

$$V_T \sim I_C R_n. \quad (2)$$

Both results (1) and (2) are due to the presence of nonequilibrium low-energy quasiparticles (which arise from the normal terminals) suffering little dephasing while propagating across the system.

FIG. 1.  $X$ -junction structure under consideration.

*The model and basic formalism.* We will consider the structure displayed in Fig. 1: It consists of two superconducting and two normal terminals interconnected by four normal metallic wires of lengths  $L_{S_{1,2}}, L_{N_{1,2}}$  (being much shorter than the inelastic relaxation length), and cross sections  $\mathcal{A}_{S_{1,2}}, \mathcal{A}_{N_{1,2}}$ , respectively. For brevity in what follows, we will denote this structure as the  $X$  junction. The superconducting terminals are biased by the phase twist  $\chi = \chi_1 - \chi_2$  and the supercurrent  $I_S(\chi)$  can flow between these terminals for nonzero  $\chi$ . The two normal terminals are disconnected from any external circuit and are maintained at different temperatures  $T_1$  and  $T_2$ .

In order to proceed we will make use of the standard quasiclassical formalism of the Usadel equations [5]

$$iD\nabla(\check{G}\nabla\check{G}) = [\hat{\Omega}\check{1}, \check{G}], \quad \check{G}\check{G} = \check{1}, \quad (3)$$

which allow us to evaluate the  $4 \times 4$  Green-Keldysh matrix functions  $\check{G} = \begin{pmatrix} \hat{G}^R & \hat{G}^K \\ 0 & \hat{G}^A \end{pmatrix}$  for our  $X$  junction. Here,  $D$  stands

for the diffusion constant, and  $\hat{G}^{R,A} = \begin{pmatrix} G^{R,A} & F^{R,A} \\ \tilde{F}^{R,A} & -G^{R,A} \end{pmatrix}$  are retarded and advanced  $2 \times 2$  Green's function matrices in the Nambu space,  $\hat{\Omega} = \begin{pmatrix} \varepsilon + eV & \Delta \\ -\Delta^* & -\varepsilon + eV \end{pmatrix}$ , where  $\varepsilon$ ,  $V$ , and  $\Delta$  denote, respectively, the quasiparticle energy, electrostatic potential, and superconducting order parameter. The Keldysh matrix has the form  $\hat{G}^K = \hat{G}^R \hat{h} - \hat{h} \hat{G}^A$ , where  $\hat{h}$  is the matrix distribution function. The current density  $\mathbf{j}$  is expressed by means of the standard relation

$$\mathbf{j} = -\frac{\sigma}{8e} \int d\varepsilon \text{tr} (\hat{\tau}_3 \check{G} \nabla \check{G})^K, \quad (4)$$

where  $\sigma$  is the normal Drude conductivity and  $\hat{\tau}_3$  is one of the Pauli matrices in the Nambu space.

It is convenient to decompose the matrix distribution function as  $\hat{h} = h^L + \hat{\tau}_3 h^T$ . In the normal wires the functions  $h^L$  and  $h^T$  obey the diffusionlike equations

$$iD\nabla[D^T \nabla h^T + \mathcal{Y} \nabla h^L + \mathbf{j}_\varepsilon h^L] = 0, \quad (5)$$

$$iD\nabla[D^L \nabla h^L - \mathcal{Y} \nabla h^T + \mathbf{j}_\varepsilon h^T] = 0. \quad (6)$$

Here,  $D^{T/L} = v^2 \pm |F^R \pm F^A|^2/4$  defines the two kinetic coefficients and  $v = \text{Re } G^R$  is the local electron density of states. The third kinetic coefficient  $\mathcal{Y} = (|\tilde{F}^R|^2 - |F^R|^2)/4$  accounts

for the presence of particle-hole asymmetry in our system and

$$\mathbf{j}_\varepsilon = \frac{1}{2} \text{Re}(F^R \nabla \tilde{F}^R - \tilde{F}^R \nabla F^R) \quad (7)$$

defines the spectral current.

As usual, the above equations should be supplemented by proper boundary conditions at the intermetallic interfaces. Here, we assume that all interfaces between the wires and the terminals are fully transparent and hence the Green's functions are matched continuously at these interfaces. The same applies to the contact between the wires (point  $c$  in Fig. 1). We also assume that all four normal wires are thin enough and long enough enabling one (a) to fully ignore their effect on the bulk terminals and (b) to consider the effective Thouless energy of our device  $E_{\text{Th}} = D/L_S^2$  (with  $L_S = L_{S_1} + L_{S_2}$ ) as the only relevant energy scale in our problem. This is appropriate provided  $E_{\text{Th}} \ll |\Delta|$ . The latter inequality—combined with the condition  $T_{1,2} \ll |\Delta|$ —implies that our analysis can be restricted to subgap energies. The temperatures of the superconducting terminals are also assumed to be well below the superconducting gap, rendering them irrelevant for our further analysis.

*Long-range phase coherent thermoelectricity.* Applying a thermal gradient to normal terminals  $N_1$  and  $N_2$ , one induces thermoelectric voltages  $V_1$  and  $V_2$  at these terminals [7–13]. These voltage signals are in general not small and depend periodically on the phase  $\chi$ , as it was repeatedly observed in experiments [14–17]. Both these features are direct consequences of the particle-hole asymmetry generated by the mechanism of sequential Andreev reflection at two NS interfaces [9].

The quasiparticle distribution function inside the  $X$  junction is recovered from the diffusionlike equations (5) and (6) combined with the condition that no electric current can flow into normal terminals  $N_1$  and  $N_2$ . With this in mind, we get

$$h_{N_{1,2}}^{T/L} = \frac{1}{2} \left[ \tanh \frac{\varepsilon + eV_{1,2}}{2T_{1,2}} \mp \tanh \frac{\varepsilon - eV_{1,2}}{2T_{1,2}} \right] \quad (8)$$

at the interfaces between the N wire and the corresponding N terminal, while at both SN interfaces we have  $h^T = 0$ .

To begin with, we note that in partially symmetric  $X$  junctions with (i)  $L_{S_1} = L_{S_2} = L_S/2$  and (ii)  $\mathcal{A}_{S_1} = \mathcal{A}_{S_2}$ , the kinetic coefficient  $\mathcal{Y}$  is equal to zero in the crossing point  $c$  and everywhere in the N wires attached to normal terminals  $N_1$  and  $N_2$ . In order to prove this property, one should bear in mind that  $\mathcal{Y}$  is an *odd* function of the phase  $\chi$ . Interchanging the terminals  $S_1 \leftrightarrow S_2$  and inverting the phase sign  $\chi \rightarrow -\chi$ , under the conditions (i) and (ii) we arrive at the same  $X$  junction as the initial one. Hence, in this case,  $\mathcal{Y}$  should also be an *even* function of  $\chi$ , which is only possible if  $\mathcal{Y} \equiv 0$ .

Setting  $\mathcal{Y} = 0$  in Eqs. (5) and (6) in the wires connected to the N terminals, one may verify that  $h^T \equiv 0$  becomes a trivial solution of these equations everywhere in our system. Combining this solution with Eq. (8), we observe that both voltages  $V_{1,2}$  vanish identically in this case. Then the kinetic equations (5) and (6) reduce to  $D^L \nabla h^L = C_1$  and  $h^L = C_2$  (with  $C_1$  and  $C_2$  being constants) in the N wires connected respectively to the N and to S terminals. Resolving these equations, we recover the distribution function  $h^L$  inside the

wires attached to the superconducting terminals,

$$h^L = r_{N_2}^L h_{N_1}^L + r_{N_1}^L h_{N_2}^L, \quad (9)$$

where  $r_{N_i}^L = R_{N_i}^L / (R_{N_1}^L + R_{N_2}^L)$  and

$$R_{N_i}^L = \frac{1}{\mathcal{A}_{N_i} \sigma} \int_{L_{N_i}} \frac{dx}{D^L}, \quad i = 1, 2 \quad (10)$$

are spectral resistances of the  $N$  wires attached to the normal terminals  $N_1$  and  $N_2$ .

The above simple analysis demonstrates that no thermoelectric effect may occur in our  $X$  junction provided the kinetic coefficient  $\mathcal{Y}$  vanishes in the  $N$  wires attached to the normal terminals. We now lift the conditions (i) and (ii) and evaluate the thermoelectric voltages  $V_1$  and  $V_2$ .

The corresponding derivation is outlined in the Supplemental Material (SM) [18], and here we only quote the final result. Assuming that both temperatures strongly exceed the Thouless energy  $T_{1,2} \gg E_{\text{Th}}$ , for the thermoelectric voltage induced at the terminal  $N_1$  we obtain

$$eV_1 = \frac{r_{N_1}}{4} \left( \frac{1}{T_2} - \frac{1}{T_1} \right) \int \varepsilon d\varepsilon \int_{L_{N_1}} \mathcal{Y} \frac{dx}{L_{N_1}}, \quad (11)$$

where  $r_{N_i} = R_{N_i} / (R_{N_1} + R_{N_2})$  and  $R_{N_i} = L_{N_i} / (\mathcal{A}_{N_i} \sigma)$  ( $i=1, 2$ ) are normal-state resistances of the wires attached to normal reservoirs. The function  $\mathcal{Y}$  in Eq. (11) can be evaluated numerically or estimated analytically extrapolating the results derived in the limit  $|\varepsilon| \gg E_{\text{Th}}$  to lower energies. The latter procedure allows us to perform the integrals in Eq. (11) and get

$$eV_1 \approx \frac{\gamma \varkappa^2 r_{N_1} (L_{S_1} - L_{S_2}) E_{\text{Th}}^2}{L_{N_1} (3 + 2\sqrt{2})} \left( \frac{1}{T_2} - \frac{1}{T_1} \right) \sin \chi, \quad (12)$$

where  $\gamma = (L_S^2 + 2L_{S_1}L_{S_2})L_S^4 / (L_{S_1}^2 + L_{S_2}^2)^3$  and  $\varkappa = 4\sqrt{\mathcal{A}_{S_1}\mathcal{A}_{S_2}} / (\mathcal{A}_{S_1} + \mathcal{A}_{S_2} + \mathcal{A}_{N_1} + \mathcal{A}_{N_2})$  are dimensionless geometric factors.

Equations (11) and (12) represent the first key result of our present work. The periodic dependence of the thermoelectric signal (12) on the phase  $\chi$  demonstrates that long-range phase coherence in our  $X$  junction is well maintained even at high enough temperatures  $T_{1,2} \gg E_{\text{Th}}$ . It is also remarkable that under this condition the amplitude of the thermoinduced voltage  $V_1$  (12) decreases with increasing temperature only as a power law, i.e., much slower than it was previously reported elsewhere [7–9].

The thermoelectric voltage  $V_2$  induced at the second normal terminal  $N_2$  can be obtained from the above Eqs. (11) and (12) by interchanging the indices  $1 \leftrightarrow 2$ . In symmetric structures with  $L_{N_1} = L_{N_2}$  and  $\mathcal{A}_{N_1} = \mathcal{A}_{N_2}$ , one readily finds  $V_2 = -V_1$ .

In addition to the above analysis, we resolved the Usadel equations numerically and evaluated the thermoelectric voltages  $V_{1,2}$  employing no approximations. Our numerically exact results for  $V_1$  are displayed in Figs. 2 and 3 (solid lines) together with Eq. (11) (where  $\mathcal{Y}$  was evaluated numerically) and Eq. (12) indicated respectively by long and short dashed lines.

*Long-range Josephson effect.* We now turn to dc Josephson effect in the presence of a temperature gradient. For simplicity,

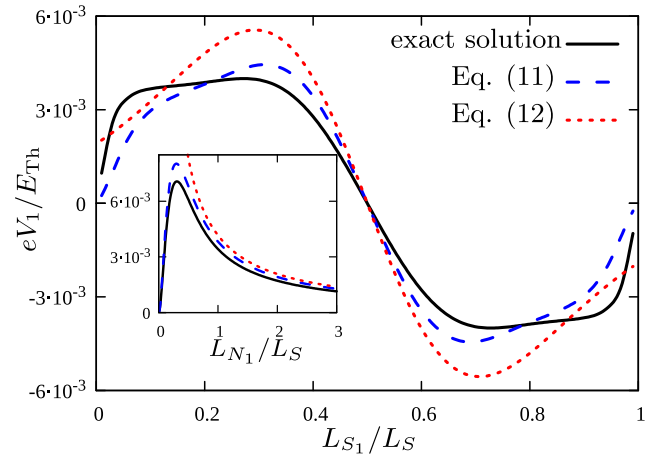


FIG. 2. Thermoelectric voltage  $V_1$  at  $\chi = \pi/2$ ,  $T_1 = 20E_{\text{Th}}$ , and  $T_2 = 30E_{\text{Th}}$  as a function of  $L_{S_1}$  for  $L_{N_1} = L_{N_2} = L_S$  and  $\mathcal{A}_{S_1} = \mathcal{A}_{S_2} = \mathcal{A}_{N_1} = \mathcal{A}_{N_2}$ . Inset: The same voltage as a function of  $L_{N_1} = L_{N_2}$  for  $L_{S_1} = 0.3L_S$ .

in what follows we again impose the symmetry conditions (i) and (ii) and denote  $\mathcal{A}_{S_{1,2}} = \mathcal{A}_S$ . As we demonstrated above, in this particular case no electron-hole asymmetry is generated and hence no thermoelectric effect occurs, i.e.  $V_{1,2} = 0$ . Furthermore, the distribution function  $h^T$  is equal to zero, while the function  $h^L$  inside the wires is defined by Eq. (9).

Let us introduce the function  $W(\varepsilon) = r_{N_2}^L r_{N_1} - r_{N_1}^L r_{N_2}$  and identically rewrite Eq. (9) in the form

$$h^L = r_{N_2} h_{N_1}^L + r_{N_1} h_{N_2}^L + W(\varepsilon)(h_{N_1}^L - h_{N_2}^L). \quad (13)$$

The first two terms on the right-hand side of Eq. (13) represent a superposition of the equilibrium distribution functions  $h_{N_1}^L$  and  $h_{N_2}^L$  with energy-independent prefactors, while the last term is essentially nonequilibrium in nature. The function  $W(\varepsilon)$  vanishes identically in structures with  $L_{N_1} = L_{N_2}$ , otherwise it remains nonzero at low enough energies and decays exponentially provided  $|\varepsilon|$  exceeds the Thouless energy of our device  $E_{\text{Th}}$ .

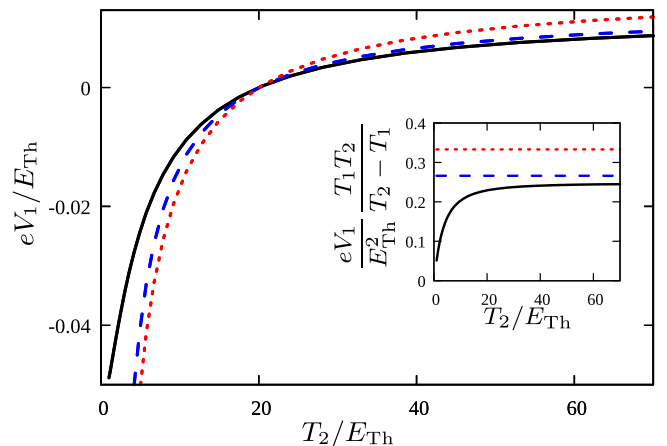


FIG. 3. Thermoelectric voltage  $V_1$  as a function of temperature  $T_2$ . The notations and the values of  $\chi$ ,  $T_1$ ,  $L_{S_1}$  are the same as in Fig. 2 and  $L_{N_1} = L_S/2$ ,  $L_{N_2} = L_S$ .

With the aid of Eq. (13), we immediately recover the expression for the supercurrent  $I_S$  flowing between the superconducting terminals  $S_1$  and  $S_2$  across the normal wire of length  $L_S$ . We obtain

$$I_S = r_{N_2} I_J(T_1, \chi) + r_{N_1} I_J(T_2, \chi) + I_S^{\text{ne}}(T_1, T_2, \chi), \quad (14)$$

where

$$I_J(T, \chi) = -\frac{\sigma A_S}{2e} \int j_\varepsilon \tanh \frac{\varepsilon}{2T} d\varepsilon \quad (15)$$

is the equilibrium Josephson current and

$$I_S^{\text{ne}} = \frac{\sigma A_S}{2e} \int j_\varepsilon W(\varepsilon) \left( \tanh \frac{\varepsilon}{2T_2} - \tanh \frac{\varepsilon}{2T_1} \right) d\varepsilon. \quad (16)$$

Equations (14)–(16) define the second key result of this work. It demonstrates that provided our  $X$  junction is biased by a temperature gradient, the supercurrent  $I_S$  consists of two different contributions. The first one is a weighted sum of equilibrium Josephson currents  $I_J$  (15) evaluated at temperatures  $T_1$  and  $T_2$  and the second one  $I_S^{\text{ne}}$  (16) accounts specifically for nonequilibrium effects.

Our numerical analysis indicates that provided at least one of the two temperatures remains below the Thouless energy  $E_{\text{Th}}$ , the current  $I_S$  (14) is dominated by the first (quasiequilibrium) contribution, while the nonequilibrium one (16) can be safely neglected. In the opposite limit  $T_{1,2} \gg E_{\text{Th}}$ , the equilibrium contribution to  $I_S$  [cf. Eq. (15)] gets exponentially suppressed as (cf. Refs. [19,20])

$$I_J = \frac{16\kappa}{3 + 2\sqrt{2}} \frac{E_{\text{Th}}}{eR_n} \left( \frac{2\pi T}{E_{\text{Th}}} \right)^{3/2} e^{-\sqrt{2\pi T/E_{\text{Th}}}} \sin \chi, \quad (17)$$

where  $R_n = L_S/(A_S \sigma)$  and the prefactor  $\kappa$  is taken at  $A_{S_{1,2}} = A_S$ . Thus, at  $T_{1,2} \gg E_{\text{Th}}$ , the supercurrent can already be dominated by the nonequilibrium term  $I_S^{\text{ne}}$ . Evaluation of the energy integral in Eq. (16) yields (see Ref. [18])

$$I_S^{\text{ne}} \simeq 0.21\kappa^3 r_{N_1} r_{N_2} \frac{E_{\text{Th}}^2}{eR_n} \left( \frac{1}{T_1} - \frac{1}{T_2} \right) \times \left( \frac{L_S}{L_{N_2}} - \frac{L_S}{L_{N_1}} \right) \sin \chi \cos^2(\chi/2). \quad (18)$$

This result is remarkable in several important aspects. First of all, we observe that at temperatures strongly exceeding the Thouless energy, the supercurrent  $I_S \simeq I_S^{\text{ne}}$  decays with increasing  $\min(T_1, T_2)$  only as a power law, in contrast to the equilibrium Josephson current in long SNS junctions which is known to decay exponentially. This behavior is due to driving the electron distribution function  $h^L$  out of equilibrium by applying a temperature gradient. In Figs. 4 and 5 we show the critical Josephson current  $I_C$  as a function of  $T_2$  for fixed  $T_1$ . We indeed observe that at large temperatures,  $T_2 \gg E_{\text{Th}}$ ,  $I_C$  significantly exceeds both equilibrium values  $I_J(T_1)$  and  $I_J(T_2)$  and even starts to grow for  $T_2 \gtrsim T_1$ . Hence, we predict *strong supercurrent stimulation by a temperature gradient*.

Another interesting feature of the result (18) is the nonsinusoidal CPR that persists at temperatures well above  $E_{\text{Th}}$ . For comparison, the dependence of the equilibrium Josephson current on the phase  $\chi$  in SNS junctions remains nonsinusoidal only at  $T \lesssim E_{\text{Th}}$  and reduces to  $I_J \propto \sin \chi$  at higher temperatures.

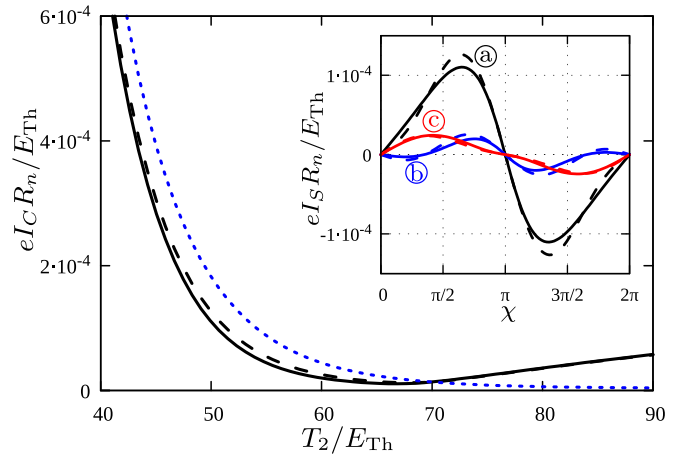


FIG. 4. Josephson critical current  $I_C \equiv \max|I_S|$  as a function of  $T_2$ . Inset: CPR evaluated at  $T_2 = 50E_{\text{Th}}$  (a),  $60E_{\text{Th}}$  (b), and  $75E_{\text{Th}}$  (c). Solid lines correspond to the exact numerical solution, dashed lines indicate the result (14) combined with (17) and (18), and the dotted line is the quasiequilibrium contribution  $r_{N_2} I_J(T_1, \pi/2) + r_{N_1} I_J(T_2, \pi/2)$  to  $I_S$ . The parameters are  $T_1 = 70E_{\text{Th}}$ ,  $L_{S_{1,2}} = L_S/2$ ,  $L_{N_1} = 3L_S$ ,  $L_{N_2} = L_S$ , and  $A_{S_1} = A_{S_2} = A_{N_1} = A_{N_2}$ .

In addition, we observe that the sign of the supercurrent in Eq. (18) is controlled by those of both length and temperature differences,  $L_{N_1} - L_{N_2}$  and  $T_1 - T_2$ . For instance, by choosing  $L_{N_1} < L_{N_2}$  and  $T_1 < T_2$  we arrive at a pronounced  $\pi$ -junction-like behavior (see also Fig. 5).

Previously switching to the  $\pi$ -junction state in a configuration similar to ours was realized by applying an external voltage bias  $V$  to normal terminals [21–24]. In this case, the electron distribution function is also driven out of equilibrium, however, unlike here, the magnitude of the supercurrent remains exponentially small for  $eV, T \gg E_{\text{Th}}$  [22]. Alternatively, by creating nonequilibrium conditions with the aid of an external rf signal, it is possible to efficiently stimulate the supercurrent in long SNS junctions [25,26]. However, no  $\pi$ -junction behavior could be obtained in this way. In contrast to

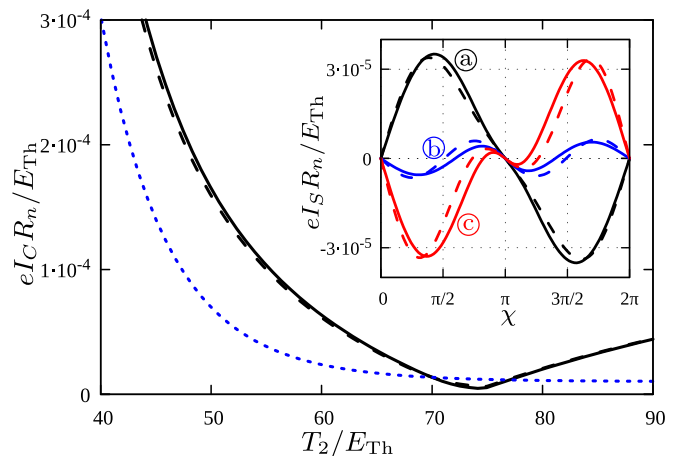


FIG. 5. The same as in Fig. 4. The parameters are the same except  $L_{N_1} = L_S$ ,  $L_{N_2} = 3L_S$ . Temperature values in the inset are  $T_2 = 65E_{\text{Th}}$  (a),  $75E_{\text{Th}}$  (b), and  $85E_{\text{Th}}$  (c).

the above examples, exposing the  $X$  junction to a temperature gradient makes both nontrivial features—supercurrent stimulation and  $\pi$ -junction states—simultaneously observable in the same experiment.

The supercurrent  $I_S$  was also evaluated numerically without employing any approximations. The corresponding results are displayed in Figs. 4 and 5 together with Eq. (14) combined with Eqs. (17) and (18). In Fig. 4 the parameters are chosen such that the nonequilibrium term  $I_S^{\text{ne}}$  remains negative for  $T_2 < T_1$ , and the  $\pi$ -junction states may only exist in a tiny interval of  $T_2$  below  $T_1$ . In contrast, in Fig. 5 the  $\pi$ -junction behavior is realized practically at any  $T_2 > T_1$  [cf. curves (b) and (c) in the inset] since the term  $I_S^{\text{ne}}$  takes negative values at such temperatures.

Note that here the transition between 0- and  $\pi$ -junction states does *not* correspond to a vanishing Josephson critical current  $I_C \equiv \max|I_S|$ . It follows from a nonsinusoidal form of CPR (18), in contrast to the standard situations. The value  $I_C$  may be achieved either at  $\chi < \pi/2$  or at  $\chi > \pi/2$  depending on whether the maximum or the minimum of  $I_S^{\text{ne}}$  (18) is reached at  $\chi = \pi/3$ . Furthermore, the competition between the terms  $\propto I_J$  and  $I_S^{\text{ne}}$  may also cause an extra maximum and minimum of the dependence  $I_S(\chi)$  [cf. curve (b) in Fig. 4

and curves (b) and (c) in Fig. 5], since in a narrow vicinity of  $\chi = \pi$  the contribution containing  $I_J \propto (\pi - \chi)$  always dominates over the nonequilibrium one,  $I_S^{\text{ne}} \propto (\pi - \chi)^3$ .

In summary, we have demonstrated that clear manifestations of long-range phase coherence may persist up to much higher temperatures as compared to  $E_{\text{Th}}$  provided our  $X$  junction is exposed to a thermal gradient. In particular, at  $T_{1,2} \gg E_{\text{Th}}$ , both the Josephson critical current  $I_C$  and the magnitude of the phase-coherent voltage signal  $V_T = \max V_{1,2}$  exhibit exactly the same algebraic dependence on  $T_1$  and  $T_2$  [cf. Eqs. (1) and (2)]. In both cases long-range phase coherence is maintained due to nonequilibrium quasiparticles with energies below  $E_{\text{Th}}$  propagating across the system without any significant phase relaxation [27]. Our results indicate that quantum properties of  $X$  junctions can be efficiently controlled and manipulated with the aid of both superconducting phase and temperature gradient, thereby opening up different opportunities for a variety of applications of such structures as central elements in superconductivity-based quantum electronics and quantum information devices.

Two of us (M.S.K. and A.D.Z.) acknowledge partial support by RFBR Grant No. 18-02-00586.

- 
- [1] V. L. Ginzburg, *Rev. Mod. Phys.* **76**, 981 (2004).  
 [2] F. Giazotto, T. T. Heikkilä, A. Luukanen, A. M. Savin, and J. P. Pekola, *Rev. Mod. Phys.* **78**, 217 (2006).  
 [3] A. Fornieri and F. Giazotto, *Nat. Nanotechnol.* **12**, 944 (2017).  
 [4] N. Li, J. Ren, L. Wang, G. Zhang, P. Hanggi, and B. Li, *Rev. Mod. Phys.* **84**, 1045 (2012).  
 [5] W. Belzig, F. K. Wilhelm, C. Bruder, G. Schön, and A. D. Zaikin, *Superlatt. Microstruct.* **25**, 1251 (1999).  
 [6] A. A. Golubov, M. Yu. Kupriyanov, and E. Il'ichev, *Rev. Mod. Phys.* **76**, 411 (2004).  
 [7] R. Seviour and A. F. Volkov, *Phys. Rev. B* **62**, R6116 (2000). An exponential decay of the thermoelectric signal with increasing  $T \gg \epsilon_L$  follows directly from Eqs. (7) and (8) of that work.  
 [8] P. Virtanen and T. T. Heikkilä, *Phys. Rev. Lett.* **92**, 177004 (2004); *J. Low Temp. Phys.* **136**, 401 (2004); *Appl. Phys. A* **89**, 625 (2007).  
 [9] M. S. Kalenkov and A. D. Zaikin, *Phys. Rev. B* **95**, 024518 (2017).  
 [10] V. R. Kogan, V. V. Pavlovskii, and A. F. Volkov, *Europhys. Lett.* **59**, 875 (2002).  
 [11] A. F. Volkov and V. V. Pavlovskii, *Phys. Rev. B* **72**, 014529 (2005).  
 [12] P. E. Dolgirev, M. S. Kalenkov, and A. D. Zaikin, *Phys. Rev. B* **97**, 054521 (2018).  
 [13] P. E. Dolgirev, M. S. Kalenkov, and A. D. Zaikin, *Phys. Status Solidi RRL* **13**, 1800252 (2019).  
 [14] J. Eom, C.-J. Chien, and V. Chandrasekhar, *Phys. Rev. Lett.* **81**, 437 (1998).  
 [15] A. Parsons, I. A. Sosnin, and V. T. Petrashov, *Phys. Rev. B* **67**, 140502(R) (2003).  
 [16] P. Cadden-Zimansky, Z. Jiang, and V. Chandrasekhar, *New J. Phys.* **9**, 116 (2007).  
 [17] C. D. Shelly, E. A. Matrozova, and V. T. Petrashov, *Sci. Adv.* **2**, e1501250 (2016).  
 [18] See Supplemental Material at <http://link.aps.org/supplemental/10.1103/PhysRevB.101.180505> for details of the calculations of the long-range thermoelectric and Josephson effects.  
 [19] A. D. Zaikin and G. F. Zharkov, *Fiz. Nizk. Temp.* **7**, 375 (1981) [*Sov. J. Low Temp. Phys.* **7**, 181 (1981)].  
 [20] P. Dubos, H. Courtois, B. Pannetier, F. K. Wilhelm, A. D. Zaikin, and G. Schon, *Phys. Rev. B* **63**, 064502 (2001).  
 [21] A. F. Volkov, *Phys. Rev. Lett.* **74**, 4730 (1995).  
 [22] F. K. Wilhelm, G. Schön, and A. D. Zaikin, *Phys. Rev. Lett.* **81**, 1682 (1998).  
 [23] S. Yip, *Phys. Rev. B* **58**, 5803 (1998).  
 [24] J. J. A. Baselmans, A. F. Morpurgo, B. J. van Wees, and T. M. Klapwijk, *Nature (London)* **397**, 43 (1999).  
 [25] L. G. Aslamazov and S. V. Lempitskii, *Zh. Eksp. Teor. Fiz.* **82**, 1671 (1982) [*Sov. Phys. JETP* **55**, 967 (1982)].  
 [26] A. D. Zaikin, *Zh. Eksp. Teor. Fiz.* **84**, 1560 (1983) [*Sov. Phys. JETP* **57**, 910 (1983)].  
 [27] This situation resembles somewhat the one encountered for the Aharonov-Bohm effect in superconducting-normal metallic heterostructures (see, e.g., Refs. [5,28,29]).  
 [28] H. Courtois, P. Gandit, D. Mailly, and B. Pannetier, *Phys. Rev. Lett.* **76**, 130 (1996).  
 [29] A. A. Golubov, F. K. Wilhelm, and A. D. Zaikin, *Phys. Rev. B* **55**, 1123 (1997).